6772 *Biochemistry* **2009,** *48,* 6772–6782
DOI: 10.1021/bi900472a

BIOCHEMISTRY
including biophysical chemistry & molecular biology
Article

Bases in 16S rRNA Important for Subunit Association, tRNA Binding, and Translocation[†]

Xinying Shi, Katie Chiu, Srikanta Ghosh, and Simpson Joseph*

Department of Chemistry and Biochemistry, University of California, San Diego, 9500 Gilman Drive, La Jolla, California 92093-0314

Received March 18, 2009; Revised Manuscript Received June 10, 2009

ABSTRACT: Ribosomes are the cellular machinery responsible for protein synthesis. A well-orchestrated step in the elongation cycle of protein synthesis is the precise translocation of the tRNA−mRNA complex within the ribosome. Here we report the application of a new in vitro modification-interference method for the identification of bases in 16S rRNA that are essential for translocation. Our results suggest that conserved bases U56, U723, A1306, A1319, and A1468 in 16S rRNA are important for translocation. These five bases were deleted or mutated so their role in translation could be studied. Depending on the type of mutation, we observed inhibition of growth rate, subunit association, tRNA binding, and/or translocation. Interestingly, deletion of U56 or A1319 or mutation of A1319 to C showed a lethal phenotype and were defective in protein synthesis in vitro. Further analysis showed that deletion of U56 or A1319 caused defects in 30S subunit assembly, subunit association, and tRNA binding. In contrast, the A1319C mutation showed no defects in subunit association; however, the extent of tRNA binding and translocation was significantly reduced. These results show that conserved bases located as far as 100 Å from the tRNA binding sites can be important for translation.

Ribosomes contain three tRNA binding sites: the aminoacyl site (A site), the peptidyl site (P site), and the exit site (E site). During protein synthesis, A and P site tRNAs move in a precise and coordinated manner to the P and E sites, respectively. Early biochemical and biophysical studies showed that the movement of the tRNAs occurs in two steps (*1*, *2*). First, following peptide bond formation, the acceptor ends of deacylated and peptidyl tRNAs translocate spontaneously into the 50S subunit's E and P sites, respectively. The anticodon ends of deacylated and peptidyl tRNAs maintain their interactions with the 30S subunit's P and A sites, respectively, resulting in hybrid P/E and A/P binding states. Second, EF-G[1] binds to the ribosome and hydrolyzes GTP. GTP hydrolysis accelerates the translocation of the anticodon end of the tRNAs and the associated mRNA by one codon relative to the 30S subunit (*3*). Recent experiments are consistent with a stepwise movement of the tRNAs through the ribosome (*4*−*10*).

Strikingly, during translocation, the ribosome goes through large-scale conformational changes as shown by cryo-electron microscopy (cryo-EM) reconstruction of stalled translocation intermediates (*11*−*14*). The changes depicted by cryo-EM showed the large and small ribosomal subunits undergoing a ratchet-like movement relative to each other during translocation. This indicates that translocation involves multiple conformational changes in both subunits. However, conformational changes in the ribosome are not well-understood, and the molecular basis of translocation is not yet clear.

Numerous studies suggest that the rRNAs play an important role during translocation. First, mutations or modifications in rRNAs confer resistance to antibiotics, such as viomycin, thiostrepton, and spectinomycin, that block specific steps in translocation (*15*−*17*). Most of these antibiotics protect nucleotides in rRNAs from chemical probes, indicating that they bind directly to the rRNAs (*18*, *19*). Indeed, this has been confirmed by recent X-ray crystallographic studies, which showed that antibiotics that inhibit translocation, such as thiostrepton, spectinomycin, and hygromycin B, mainly contact the rRNAs (*20*−*23*). Second, EF-G protects nucleotides in 23S rRNA and has been cross-linked to 23S rRNA, suggesting that contacts with the rRNAs are critical for translocation (*24*, *25*). Third, disruption of specific interactions between the tRNAs and the rRNAs inhibits translocation (*7*, *26*−*29*).

Even though high-resolution structures of the ribosome are now available, it is difficult to predict which bases in the rRNAs are important for specific steps in translation. This gap in understanding the functional significance of the structure needs to be filled by biochemical and biophysical studies that analyze interesting features revealed by the structures. However, systematically interrogating individual bases for their functional role in translation can become tedious and expensive. On the other hand, modification-interference methods allow the simultaneous

[†]This work was supported by a grant from the National Institutes of Health (GM65265 to S.J.).

*To whom correspondence should be addressed: 4102 Urey Hall, Department of Chemistry and Biochemistry, University of California, San Diego, 9500 Gilman Drive, La Jolla, CA 92093-0314. Phone: (858) 822-2957. Fax: (858) 534-7042. E-mail: sjoseph@chem.ucsd.edu.

[1]Abbreviations: EF-G, elongation factor G; GTP, guanosine 5′-triphosphate; DMS, dimethyl sulfate; CMCT, 1-cyclohexyl-3-(2-morpholinoethyl)carbodiimide metho-*p*-toluene sulfonate.

 Published on Web 06/22/2009

analysis of many residues in one experiment and have been used for identifying functionally important nucleotides in a variety of RNA structures, RNA−protein complexes, and catalytic RNAs. Specifically, modification-interference methods have proven to be useful for identifying bases in rRNA that are essential for binding of tRNA to the ribosomal A and P sites (*30*−*32*). Here, we describe a powerful in vitro modification-interference method for identifying bases in 16S rRNA that are critical for translocation. The modification-interference method is based on the site-specific cross-linking of tRNA to 16S rRNA in ribosomes that have undergone translocation. Using this modification-interference approach, 11 bases were identified that may play an important role during translocation. Interestingly, five of these bases have never been implicated as being important for translation. These five bases were mutated in the 16S rRNA, and the 16S rRNA mutants were systematically analyzed to examine their role in translation. Our results show that these bases located remotely from the tRNA binding sites affect subunit association, binding of tRNA to the P site, and translocation of the mRNA−tRNA complex by the ribosome.

EXPERIMENTAL PROCEDURES

DNA Cloning and Transcription of gene32val2 RNA. A plasmid (pG32mRNA) encoding the T7 RNA polymerase promoter and a fragment of phage T4 gene 32 mRNA from position −55 to +85 was used for constructing a mutant mRNA with a valine codon at the second position. This was accomplished by replacing the PacI−PmeI fragment with an appropriate double-stranded deoxyoligonucleotide containing a T to G transversion at the 4 position. The clone (pG32 VAL2) with a valine codon (GUU) at the second position was identified by restriction digest analysis and sequencing. Plasmid pG32 VAL2 was linearized with BamHI and used as a template for in vitro transcription using T7 RNA polymerase to generate gene32val2 mRNA.

Construction of the Defined Pretranslocation Complex. Biotin was attached to the 3′-end of deacylated *Escherichia coli* $tRNA_1^{Val}$ (Subriden) as previously described (*30*). Pretranslocation complexes were formed by activating 50 pmol of tight-couple 70S at 42 °C for 10 min in binding buffer [80 mM potassium cacodylate (pH 7.2), 20 mM magnesium acetate, and 150 mM ammonium chloride] followed by incubation at 37 °C for 10 min; 150 pmol of gene32val2 mRNA was added to the ribosomes, and the complexes were incubated at 37 °C for 6 min. Next, 100 pmol of deacylated *E. coli* $tRNA_f^{Met}$ (Sigma) was added, and the complexes were incubated at 37 °C for 30 min followed by addition of 100 pmol of 3′-biotin-$tRNA_1^{Val}$ and incubation at 37 °C for 30 min. Pretranslocation complexes (final volume of 100 μL) were placed on ice for 10 min. Pretranslocation complexes were modified by the addition of either 6 μL of kethoxal (37 mg/mL), 6 μL of DMS (1:10 dilution in 95% ethanol), or 100 μL of CMCT (42 mg/mL in binding buffer) for 10 min at 37 °C. For CMCT modification, the complexes were formed in 75 mM potassium borate (pH 7.0), 20 mM magnesium acetate, and 150 mM ammonium chloride. Reagents were removed by centrifugation in microcon 30 filtration units (Amicon) at 4 °C and concentrated to a final volume of 48 μL. In some of the experiments, $tRNA_1^{Val}$ or 3′-biotin-$tRNA_1^{Val}$ was bound directly to the ribosomal P site via omission of $tRNA_f^{Met}$ during complex formation.

Selection of 16S rRNAs from Post-Translocation Complexes. Translocation was initiated by the addition of 50 pmol (1 μM) of EF-G and 120 μM GTP (final concentration) to 48 μL of the modified pretranslocation complexes and incubation at 37 °C for 5 min. The reaction mixtures were transferred to a 96-well plate that was placed on crushed ice and irradiated with ultraviolet light with a wavelength of 312 nm (8000 μw/cm^2 intensity) for 10 min. Preliminary experiments indicated that this was sufficient to generate enough cross-linked material for streptavidin capture and primer extension analysis without damaging the ribosomes. The samples were extracted four times with water-saturated phenol followed by three chloroform extractions, and the rRNAs were recovered by ethanol precipitation (*33*). The rRNAs were resuspended in 250 μL of water (total rRNA population). 16S rRNAs, cross-linked to 3′-biotin-$tRNA_1^{Val}$, were captured using magnetic streptavidin beads (streptavidin-M280, Dynal). The beads were prewashed to remove ribonucleases as recommended by the manufacturer. Next, 125 μL of the total rRNA mixture was gently mixed with 100 μL of streptavidin beads, and the samples were processed

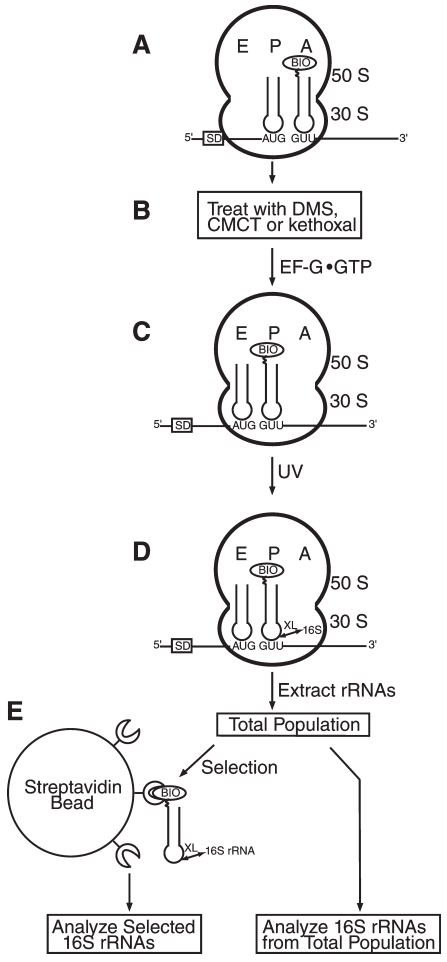

FIGURE 1: Schematic illustration of the modification-interference method. (A) Pretranslocation complex programmed with gene32val2 mRNA and having $tRNA_f^{Met}$ and 3′-biotin-$tRNA_1^{Val}$ in the P and A sites, respectively. (B) Chemical modification of the complex using DMS, CMCT, or kethoxal. (C) Translocation, catalyzed by EF-G·GTP, results in the movement of 3′-biotin-$tRNA_1^{Val}$ from the ribosomal A site to the P site. (D) Ultraviolet light induces a cross-link between 3′-biotin-$tRNA_1^{Val}$ and 16S rRNA only in the post-translocation complexes. (E) The rRNAs are extracted from the ribosomes, and the 16S rRNAs cross-linked to 3′-biotin-$tRNA_1^{Val}$ are captured using magnetic streptavidin beads. The 16S rRNAs from the total population and the selected subpopulation are analyzed in parallel by primer extension. Abbreviations: BIO, biotinyl group; XL, cross-link; SD, Shine-Dalgarno sequence.

using the manufacturer's supplied instruction. The beads were resuspended in 60 μL of water (selected 16S rRNA population). The levels of modification within the 16S rRNAs from the total and selected populations were examined by primer extension analysis as previously described (*33*). All experiments were repeated independently at least three times, and the modification levels were quantified using a Phosphorimager (Molecular Dynamics). The values were normalized for sample loading differences, and the background level estimated from the unmodified control lane was subtracted.

Toeprinting Assay. Pretranslocation complexes were formed as described above, and translocation was monitored by the toeprinting assay as described previously (*34*).

Site-Directed Mutagenesis of 16S rRNA. Site-directed mutagenesis was performed with a Quick Change PCR mutagenesis kit (Stratagene). Plasmid pKK3535 was used as a template for introducing mutations U56A, U723A, A1306U, A1319C, and A1468U into 16S rRNA. All the remaining mutations and deletions were made using plasmid pLK35-16S-MS2 to facilitate purification of lethal mutants using the MS2 affinity tag method (*29*, *35*). All clones were verified by automated DNA sequencing of the entire 16S rRNA operon.

Plasmid-Replacement Strategy. Plasmid replacement was performed as described previously (*36*, *37*). Briefly, *E. coli* strain SQZ10 (Δ7rrn) containing plasmid pHK-rrnC^{+}sacB (kanamycin resistant) was transformed with pKK3535 or pLK35-16S-MS2 containing the desired mutations. The transformants were grown overnight in LB medium (10 g of tryptone, 5 g of yeast extract, and 10 g of NaCl per liter of medium) with 100 μg/mL ampicillin at 37 °C with shaking. The cultures were diluted and plated on 2YT agar plates with 8% sucrose and 100 μg/mL ampicillin. The colonies on the plates were screened for sensitivity to kanamycin by replica plating. Plasmid replacement was confirmed by isolating plasmids and automated DNA sequencing. Cell stocks were prepared in 15% glycerol and stored at −80 °C.

Growth Curve. Growth of plasmid-replaced *E. coli* strain SQZ10 (Δ7rrn) expressing wild-type or mutant 16S rRNA occurred in 200 μL of LB medium in the presence of 100 μg/mL ampicillin at 37 °C with continuous shaking in a plate reader (Genios, Tecan). Each culture was inoculated with the same number of cells from overnight starter cultures. The absorbance at 600 nm was automatically measured every 10 min by the plate reader. The data were fit to an exponential growth curve equation ($Y = Ae^{bx}$), and the doubling time was calculated as $\ln(2)/b$ using Prism (GraphPad Prism, San Diego, CA).

Polysome Profile. Polysome profiles of *E. coli* strain SQZ10 (Δ7rrn) expressing wild-type or mutant 16S rRNA were determined essentially as described previously (*38*). Briefly, 100 mL of plasmid-replaced SQZ10 cells was grown at 37 °C in the presence of 100 μg/mL ampicillin until the absorbance at 600 nm was 0.5. Then, 400 μg of chloramphenicol (final concentration) was added to the cell culture and the culture immediately placed on ice. Cells were harvested and resuspended in 500 μL of 20 mM Tris (pH 7.5) and 15 mM $MgCl_2$. The cells were then lysed with lysozyme (1 mg/mL final concentration) and two freeze−thaw cycles in a dry ice/ethanol bath. Then 25 μL of 10% deoxycholate (sodium salt) was added, and the cell extracts were incubated on ice for 20 min. The absorbance of the extracts was measured at 260 nm, and 0.6 mg of ribosome equivalent was loaded onto a 10 to 40% sucrose gradient containing 20 mM Tris (pH 7.5), 10 mM $MgCl_2$, 100 mM NH_4Cl, and 2 mM β-mercaptoethanol. The samples were fractionated by ultracentrifugation at 35000 rpm for 4 h, and the gradients were profiled at 254 nm using a UA6 detector (ISCO).

Purification of MS2-Tagged 30S Subunits and Subunit Association. Mutations U56Δ, A1319Δ, and A1319C are lethal and were purified from pop 2136 cells using the MS2 affinity tag. Expression and purification were performed as described previously (*39*). The purity of the MS2-tagged preparations was assayed by primer extension after total RNA extraction. Reverse transcription using the primer 5′-CCCGTCCGCCACTCGTCAGC-3′ and NTP(-dCTP) with ddCTP gave different products for tagged and untagged 16S rRNA.

We conducted subunit association by incubating a 1.5-fold excess of 50S subunits over 30S in polyamine buffer [20 mM Hepes-KOH (pH 7.6), 6 mM $MgCl_2$, 150 mM NH_4Cl, 4 mM β-mercaptoethanol, 0.05 mM spermine, and 2 mM spermidine] (*40*, *41*), but with 20 mM $MgCl_2$ for 10 min at 42 °C, slowly cooling the mixture to 37 °C, and holding it for an additional 15 min at 37 °C. The solution was diluted with the same buffer with no $MgCl_2$ to lower its concentration to 6 mM and further incubated for an additional 15 min at 37 °C. For analyzing subunit association by sucrose gradient centrifugation, we tested different concentrations of $MgCl_2$ ranging from 10 to 20 mM. The sucrose gradients were prepared in 50 mM Tris-HCl (pH 7.6), 100 mM NH_4Cl, and 6 mM β-mercaptoethanol with 10 or 20 mM $MgCl_2$.

Two-Dimensional Gel Electrophoresis. Ribosomal proteins from the 30S subunits were isolated by acetic acid extraction as described previously (*42*), suspended in 10 μL of loading buffer containing 8 M urea, 1% 2-mercaptoethanol, and 10 mM Bis-tris acetate (pH 4.1), and analyzed by two-dimensional gel electrophoresis (*43*). The proteins were visualized after being stained with 0.25% Coomassie brilliant blue. The gels were scanned at 600 dpi and the proteins quantified using ImageOne (Bio-Rad).

In Vitro Translation of Reporter Protein. The activity of the purified ribosomes was analyzed by in vitro translation of the reporter protein Renilla luciferase as described previously (*29*). Briefly, activated ribosomes were added to the S-100 in vitro translation mix and transferred to a 96-well plate. The 96-well plate was incubated at 37 °C in a plate reader (Genios, Tecan), and the synthesis of the luciferase enzyme was monitored in real time by measuring the luminescence every 2 min. Duplicates of the samples were used for each experiment, and the assays were repeated at least two times.

tRNA Binding. We used the toeprinting assay for determining the binding of $tRNA^{fMet}$ to the P site (*44*). Briefly, activated 30S subunits (final concentration of 0.4 μM) in polyamine buffer was incubated for 10 min at 37 °C with the gene32 mRNA fragment (0.8 μM final concentration) having the AL2 primer annealed to the 3′-end. Then aliquots of the 30S mRNA mix were added to tubes containing different amounts of $tRNA^{fMet}$ (0−4 μM final concentration) prepared in polyamine buffer. The tubes were incubated at 37 °C for 30 min to allow binding of $tRNA^{fMet}$ to the P site. The complexes were analyzed by extending the AL2 primer with reverse transcriptase and separating the products on denaturing polyacrylamide gels. The toeprints were quantified with a phosphorimager, as previously described (*34*). The amount of tRNA bound = bound/(free + bound) (*44*).

We used filter binding as a second method to quantify the amount of $tRNA^{fMet}$ bound to the 30S subunits (*28*). Filter binding experiments were performed in 80 mM potassium cacodylate (pH 7.2), 7 mM $MgCl_2$, and 150 mM NH_4Cl because

the presence of polyamines increased the nonspecific background counts.

Translocation Kinetics. Rapid kinetic experiments were performed essentially as described previously (*45*). The experiments were conducted at 25 °C in polyamine buffer. Briefly, 80 μL of pretranslocation complex (0.25 μM, after mixing) containing $tRNA_f^{Met}$ and fMet-Phe-$tRNA^{Phe}$ in ribosomal P and A sites, respectively, and pyrene-labeled mRNA+9 was rapidly mixed with 80 μL of EF-G·GTP (1.25 μM, after mixing) using a stopped-flow instrument (μSFM-20, BioLogic). The samples were excited at 343 nm, and the change in fluorescence emission intensity at 376 nm was measured after the emission had passed through a long-pass filter (361 AELP, Omega Optical). Approximately five traces were averaged for each experiment, and the experiments were repeated four times. The decreases in fluorescence intensity were analyzed by nonlinear least-squares fitting to the double-exponential equation $Y = ax + b + A_1 \exp(-k_1 x) + A_2 \exp(-k_2 x)$ using Bio-Kine (BioLogic).

RESULTS

Modification-Interference Analysis. More than three decades ago, Ofengand, Zimmerman, and co-workers identified a site-specific cross-link formed between nucleotide cmo^5U34 of P site-bound $tRNA_1^{Val}$ and C1400 of 16S rRNA (*46*, *47*). This cross-link was formed in high yield (up to 70%) when the complex was irradiated with ultraviolet light from 300 to 400 nm (*47*). *E. coli* $tRNA_1^{Val}$ and $tRNA_1^{Ser}$ formed the cross-link, while $tRNA_f^{Met}$, $tRNA^{Phe}$, and $tRNA_2^{Val}$ did not form the cross-link (*47*). We repeated some of these experiments before setting up our in vitro selection method (Figure 1 of the Supporting Information). Consistent with previous studies, $tRNA_1^{Val}$ formed the cross-link to nucleotide C1400 of 16S rRNA when bound to the ribosomal P site, while $tRNA_f^{Met}$ did not form this cross-link (*47*) (Figure 1A of the Supporting Information). No cross-link was observed when $tRNA_1^{Val}$ was bound to the ribosomal A site (Figure 1B of the Supporting Information). This is in agreement with a previous report that a high salt concentration (150 mM ammonium chloride) represses cross-linking to the A site (*47*). To facilitate selection, biotin was attached to the 3′-terminus of *E. coli* $tRNA_1^{Val}$. Attachment of biotin to the 3′-terminus of $tRNA_1^{Val}$ does not strongly affect the formation of the cross-link (Figure 1C of the Supporting Information). Furthermore, only 16S rRNAs cross-linked to 3′-biotin-$tRNA_1^{Val}$ were captured by the streptavidin beads, while 16S rRNAs cross-linked to $tRNA_1^{Val}$ without the 3′-biotin do not bind to the streptavidin beads (data not shown). Thus, 16S rRNAs cross-linked to 3′-biotin-$tRNA_1^{Val}$ bind to the streptavidin beads only through the biotin moiety. Finally, $tRNA_1^{Val}$ and 3′-biotin-$tRNA_1^{Val}$ both translocate efficiently from the ribosomal A site to the P site (Figure 1D of the Supporting Information). These features of the cross-link make it suitable for the efficient isolation of 16S rRNA from ribosomes that have undergone translocation as described below.

Pretranslocation complexes were formed by programming *E. coli* ribosomes with a defined mRNA sequence and deacylated $tRNA_f^{Met}$ and 3′-biotin-$tRNA_1^{Val}$ in the P and A sites, respectively (Figure 1A). The complexes were treated with base-specific reagents dimethyl sulfate (DMS), 1-cyclohexyl-3-(2-morpholinoethyl)carbodiimide (CMCT), or kethoxal that modify rRNAs within the ribosome (Figure 1B). Treated pretranslocation complexes were incubated with EF-G·GTP to catalyze translocation.

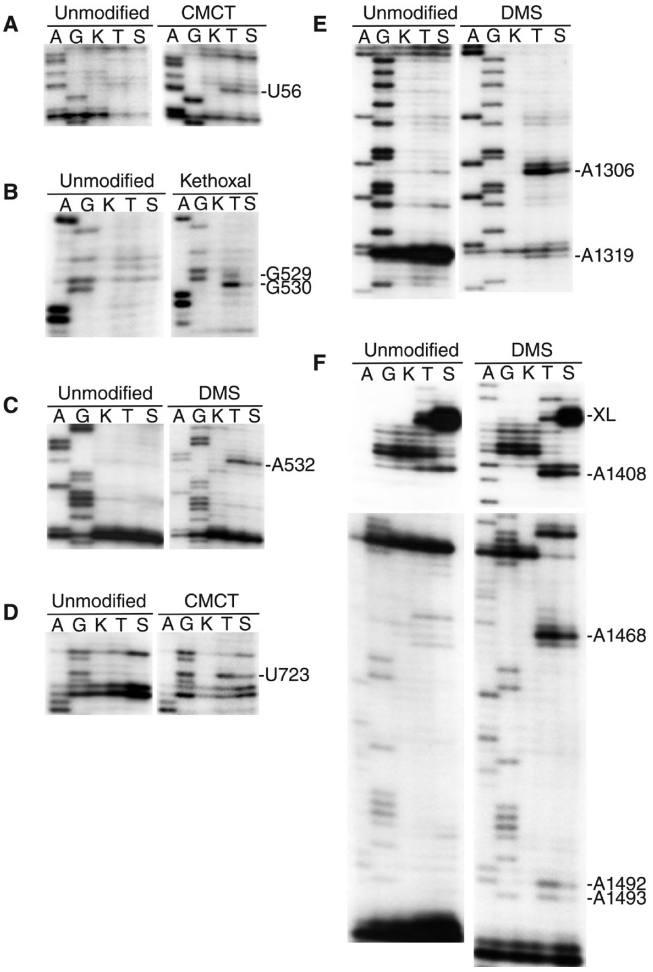

FIGURE 2: Base modifications of 16S rRNA that interfere with EF-G-dependent translocation. RNA was extracted from the ribosome and the level of modification analyzed by primer extension. rRNA from unmodified ribosomes was analyzed in parallel with either CMCT-, kethoxal-, or DMS-treated ribosomes. A and G, dideoxy sequencing lanes; K, unmodified 16S rRNA; T, 16S rRNA from the total population; S, 16S rRNA from the streptavidin-captured subpopulation. The autoradiographs show regions of 16S rRNA around (A) position 56 (CMCT), (B) position 530 (kethoxal), (C) position 532 (DMS), (D) position 723 (CMCT), (E) positions 1306−1319 (DMS), and (F) positions 1400−1493 (DMS).

Translocation resulted in the movement of $tRNA_f^{Met}$ and $tRNA_1^{Val}$ into the E and P sites, respectively (Figure 1C). However, a fraction of the ribosomes do not undergo translocation due to the modification of bases in 16S rRNA that are important for translocation. To identify these bases that are important for translocation, we irradiated the reaction mixture with ultraviolet light to form the site-specific cross-link between P site-bound 3′-biotin-$tRNA_1^{Val}$ and 16S rRNA (Figure 1D). This cross-link occurred only in ribosomes that have undergone translocation because they contain the 3′-biotin-$tRNA_1^{Val}$ properly positioned in the P site. The samples were extracted using phenol and chloroform and the rRNAs recovered by ethanol precipitation. 16S rRNAs cross-linked to 3′-biotin-$tRNA_1^{Val}$ were captured using magnetic streptavidin beads, and the rRNAs were analyzed by primer extension (Figure 1E). Bases that are critical for translocation were identified by comparing the modification levels in the total population versus the selected subpopulation. Bases that are important for translocation lost their functional competence by the modification and

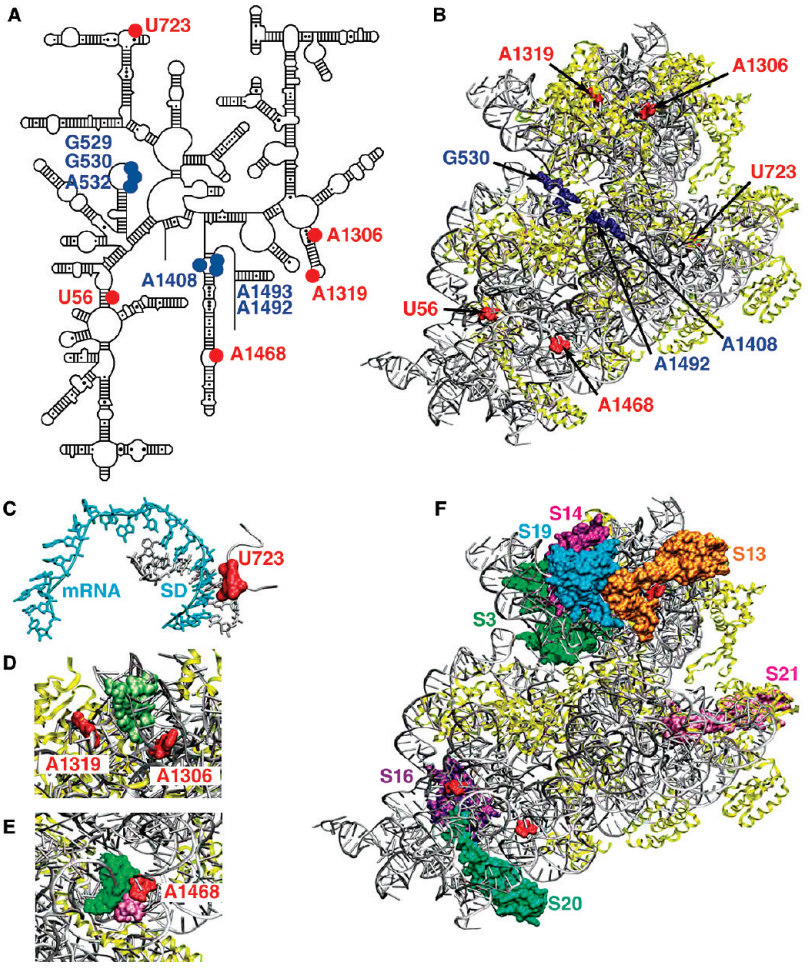

FIGURE 3: Location of the nucleotides identified by the modification-interference method. (A) Bases that are protected by A site tRNA (blue) and bases newly identified (red) are indicated on the secondary structure of 16S rRNA. (B) Three-dimensional location of nucleotides in the X-ray crystal structure of the *E. coli* 30S subunit (Protein Data Bank entry 2AVY). The 16S rRNA and the r-proteins are colored silver and yellow, respectively. (C) Base U723 interacts with the minor groove of the Shine-Dalgarno helix (Protein Data Bank entry 2QNH). mRNA is colored cyan and 16S rRNA (1539−1541) silver. (D) Tertiary interactions between helix 41 (A1268 and G1269) and helix 42 (base pairs A1311-U1326 and G1312-C1325) are colored green. (E) Tertiary interactions between helix 13 [U317 to A336 (green)] and helix 44 [A1433 and A1434 (mauve)]. (F) Ribosomal proteins in the vicinity of the selected bases. Proteins S16 (violet) and S20 (green) are located close to U56 in the "body" of the 30S subunit. Proteins S3 (dark green), S13 (orange), S14 (magenta), and S19 (cyan) are located close to A1306 and A1319 in the "head" of the 30S subunit. Protein S21 (mauve) is located close to U723 in the "platform" of the 30S subunit. The figures were created using VMD and rendered using POV-Ray.

therefore are underrepresented in the 16S rRNA from post-translocation ribosomes captured by the cross-link to 3′-biotin-$tRNA_1^{Val}$.

Primer extension analysis revealed a decreased level of modification of nucleotides U56, G529, G530, A532, U723, A1306, A1319, A1408, A1468, A1492, and A1493 in 16S rRNA from the selected subpopulation (Figure 2). Positions G529, G530, A532, A1408, A1492, and A1493 correspond to the class I sites that are protected when tRNA is bound to the ribosomal A site (*48*). These bases were anticipated to show up in the experiment because the ribosome population is never 100% active in binding tRNAs, and these A site residues are modified in ribosomes with a vacant A site. Only ribosomes that had a tRNA bound to the A site translocated. The selected 16S rRNAs, therefore, showed the characteristic A site protection pattern. This result confirms that only ribosomes that contain a tRNA in the A site were competent in translocation. Furthermore, the streptavidin-captured 16S rRNA subpopulation showed a substantial enrichment for the C1400 cross-linked product compared to the total population, thereby validating the selection scheme (Figure 2F). In addition to the class I sites, bases U56, U723, A1306, A1319, and A1468 were identified by the modification-interference method (Figure 3A,B).

Site-Directed Mutagenesis of 16S rRNA Bases. Bases in 16S rRNA that are protected by A site tRNA have been the subject of mutational analysis by several groups and were not analyzed further. The other five bases (U56, U723, A1306, A1319, and A1468) in 16S rRNA identified in this study have not been analyzed by mutational studies. To analyze the role of these 16S rRNA bases in translation, we introduced transition, transversion, and deletion at each position by site-directed mutagenesis. Mutant plasmids were introduced into *E. coli* strain SQZ10 (Δ7rrn) in which all seven copies of the rRNA operons have been deleted from the chromosome (*36*, *37*). *E. coli* strain SQZ10 (Δ7rrn) survives by expressing the wild-type rRNA genes from a resident plasmid. After several generations, most of the mutant plasmids were able to replace the resident plasmid, indicating that the mutations are not lethal to the cell. However, plasmids with U56Δ, A1319C, or A1319Δ mutations were unable to replace the resident plasmid, indicating that these mutations are lethal.

Table 1: Growth Rates of *E. coli* Expressing Mutant 16S rRNAs

ribosome	doubling time[c] (min)
wild type[a]	41 ± 1
U56G[a]	68 ± 4
A1306Δ[a]	80 ± 2
A1306C[a]	81 ± 4
A1468Δ[a]	60 ± 1
wild type[b]	61 ± 3
A1468U[b]	100 ± 5

[a] Plasmid pLK35 was used to express rRNAs. [b] Plasmid pKK3535 was used to express rRNAs. [c] The means ± standard deviations of 10 growth curves are indicated.

We next analyzed the growth rate of *E. coli* strain SQZ10 (Δ7rrn) having mutant plasmids in liquid cultures under exponential growth conditions. Mutations U56G, A1306C, A1306Δ, A1468U, and A1468Δ reduced the growth rate (Table 1), while other mutations at these positions and at U723 did not affect the growth rate (data not shown). We focused our studies on the mutations that were lethal or affected the growth rate to improve our understanding of the role of these 16S rRNA bases in protein synthesis.

Mutations Reduced the Level of Polysome Formation and Affected Subunit Association. We examined the polysome profile of *E. coli* strain SQZ10 (Δ7rrn) expressing the mutant 16S rRNAs to identify potential defects in 30S subunit assembly and subunit association. Cell extracts were fractionated on sucrose gradients to monitor the relative amounts of 30S subunits, 50S subunits, 70S ribosomes, and polysomes (Figure 4). The peaks corresponding to the polysome fractions were slightly reduced in U56G cells relative to those of wild-type cells, suggesting minor defects, if any, in 30S subunit assembly or subunit association (Figure 4B). Since U56Δ does not support the growth of *E. coli* strain SQZ10 (Δ7rrn), we cannot directly examine the polysome profile of U56Δ ribosomes. Therefore, U56Δ mutant 30S subunits were purified using an MS2 affinity tag from *E. coli* pop 2136 cells (*35*). In vitro subunit association experiments with purified U56Δ 30S subunits were performed to identify potential defects in 70S ribosome formation. Mutant 30S subunits were incubated with wild-type 50S subunits followed by ultracentrifugation in a sucrose gradient to separate the 30S and 50S subunits, and the 70S ribosome. Wild-type 30S subunits readily associated with 50S subunits to form 70S ribosomes (Figure 4G). In contrast, U56Δ 30S subunits failed to associate with the 50S subunits to form 70S ribosomes (Figure 4H).

Cells expressing A1306Δ showed a reduced amount of polysomes, and the peak corresponding to the 70S ribosome was smaller than the 50S subunit peak, indicating that this mutant is unable to efficiently form polysomes (Figure 4C). In addition, the peak corresponding to the 30S subunit was bifurcated, suggesting potential defects in 30S subunit assembly. The polysome profile for A1306C was similar to that of A1306Δ, although the 70S peak was larger in this mutant, suggesting that A1306C is not as defective as A1306Δ (Figure 4D).

We analyzed the lethal mutants A1319Δ and A1319C via the in vitro subunit association experiments. These studies showed that A1319Δ is defective in subunit association (Figure 4I). In contrast, A1319C was able to associate with the 50S subunits to form 70S ribosomes (Figure 4J). Finally, the polysome profile of A1468Δ and A1468U showed very few polysomes, and the 70S peak was significantly reduced compared to that of the wild-type

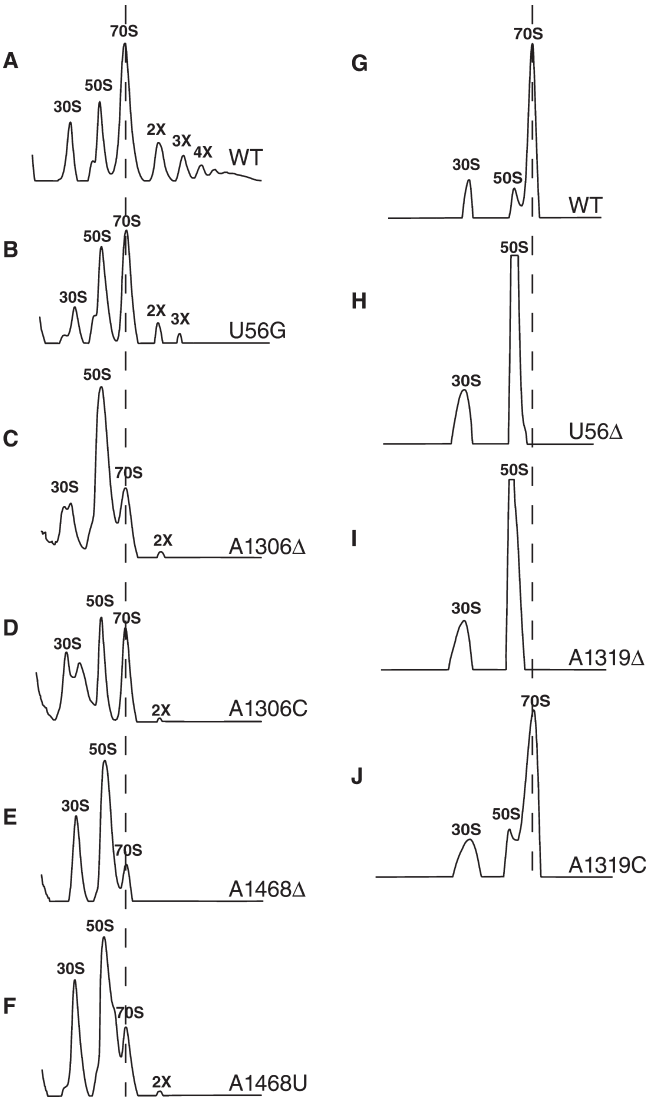

FIGURE 4: Polysome profile of cells expressing mutant 16S rRNA and subunit association. Polysome profile of cells expressing mutant 16S rRNA in *E. coli* strain SQZ10 (Δ7rrn): (A) wild-type control, (B) U56G, (C) A1306Δ, (D) A1306C, (E) A1468Δ, and (F) A1468U mutant 16S rRNA. Labels: 30S, small ribosomal subunits; 50S, large ribosomal subunits; 70S, ribosomes; 2X to 4X, polysomes. The dotted line indicates the position of the 70S ribosome in the gradients. In the case of lethal mutations, association of 30S subunits with the 50S subunits to form 70S ribosomes was analyzed by sucrose gradient centrifugation: (G) wild-type control, (H) U56Δ, (I) A1319Δ, and (J) A1319C mutant 30S subunits. The experiment was performed in buffer containing 20 mM $MgCl_2$. Labels are as described above.

strain (Figure 4E,F). Additionally, the 30S and 50S subunit peaks were larger than the 70S peak in both mutants, indicating that this base is important for 70S formation.

To understand the reason for the severe subunit association defect observed with U56Δ and A1319Δ, we analyzed the ribosomal protein (r-protein) content of the 30S subunits by two-dimensional gel electrophoresis (2D gel). 2D gel analysis showed that U56Δ 30S subunits contain reduced amounts of S2, S5, S10, S11, S12, S18, and S21 [at least 2-fold smaller amounts of r-protein than control (Figure 2D of the Supporting Information)]. In contrast, U56G 30S subunits had normal levels of r-proteins (Figure 2B of the Supporting Information). Both A1319Δ and A1319C mutants showed reduced amounts of S3, S10, S13, S14, and S18 (Figure 2E,F of the Supporting Information). However, levels of proteins S3 and S14 were significantly

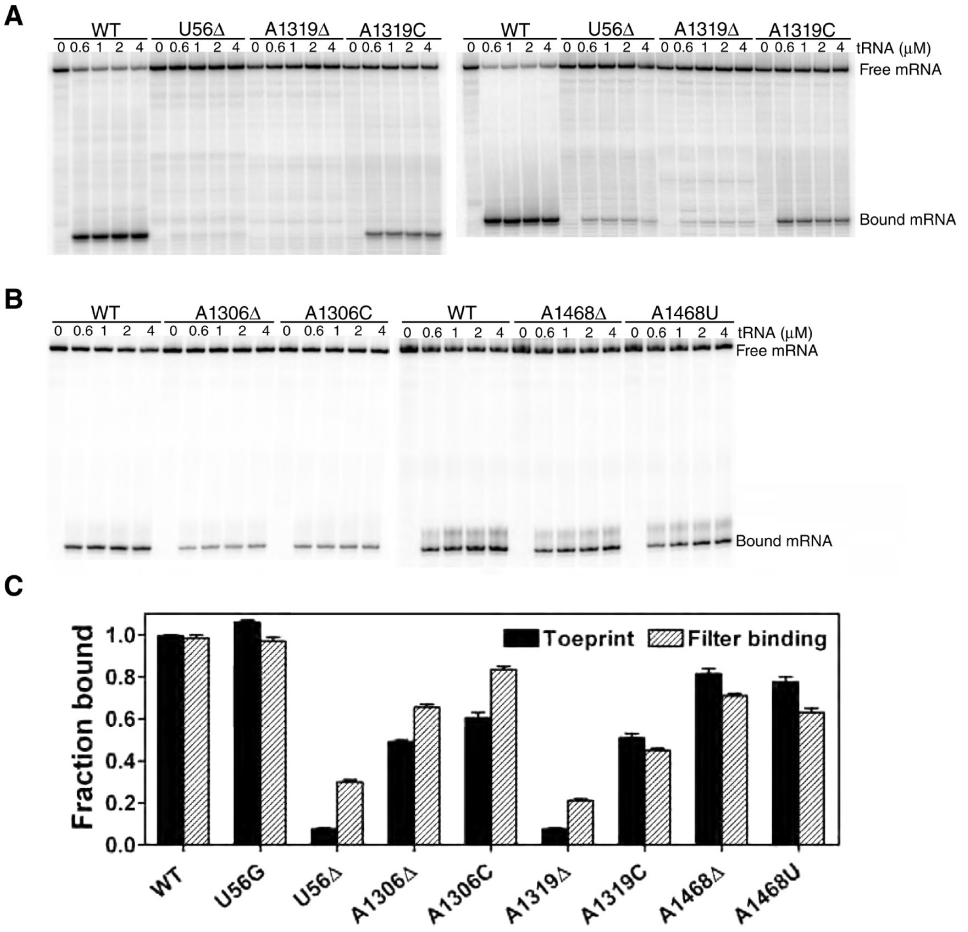

FIGURE 5: Binding of tRNA to the mutant 30S subunits. Toeprinting assay for monitoring binding of $tRNA^{fMet}$ to the ribosomal P site. (A) Binding of tRNA to the 30S subunit (left) and to the 70S ribosome (right) for mutations that cause a lethal phenotype. The final concentrations of tRNAs in the reaction are indicated above the lanes. The toeprints corresponding to the full-length cDNA (free mRNA) and mRNA bound to the 30S subunit are indicated. (B) Binding of tRNA to mutant 30S subunits purified from *E. coli* strain SQZ10 (Δ7rrn). Labels are as described above. (C) Graph showing the fraction of $tRNA^{fMet}$ bound to the 30S subunit P site. The toeprinting data are indicated by the black bars, and the filter binding data are indicated by the striped bars. The standard deviations from at least two experiments are shown.

more reduced in A1319Δ than in A1319C. S3, S13, and S14 are located close to A1319 in the ribosome structure (Figure 3F). The loss of additional r-proteins may be due to secondary effects during subunit assembly. Thus, the absence of some of these r-proteins suggests defects in the assembly of the 30S subunit, which may explain the inability of some of these mutant 30S subunits to associate with the 50S subunit to form 70S ribosomes.

Inhibition of in Vitro Protein Synthesis. Even though most of the mutations showed varying degrees of defects in the polysome profiles, they supported the growth of *E. coli* strain SQZ10 (Δ7rrn), suggesting that the mutant ribosomes are functional in vivo. We, therefore, tested whether purified mutant ribosomes are functional by examining their ability to synthesize the reporter protein Renilla luciferase using an in vitro translation assay. Synthesis of Renilla luciferase was monitored in real time by the luminescence produced when the substrate coelentrazine is hydrolyzed. The extent of synthesis of luciferase was slightly reduced with U56G ribosomes, which agrees with the modest effects on growth (Figure 3A of the Supporting Information). In contrast, U56Δ ribosomes produced very little luminescence, indicating that they are essentially inactive in this assay (Figure 3B of the Supporting Information). This is consistent with the severe subunit association defect observed for U56Δ and the inability to support growth of *E. coli* strain SQZ10 (Δ7rrn). A1306C showed no defects in the in vitro translation assay, while A1306Δ showed reduced activity. The activity of A1319C was significantly reduced, and A1319Δ was essentially inactive (Figure 3B of the Supporting Information). A1319Δ is defective in subunit association. Interestingly, however, A1319C which did not show a significant subunit association defect showed reduced in vitro translation activity. A1319C may potentially be inhibited at a step following subunit association. Finally, although both A1468Δ and A1468U exhibited a reduced level of polysomes, only A1468U exhibited inhibition in protein synthesis (Figure 3A of the Supporting Information).

Inhibition of tRNA Binding. The in vitro translation assay showed that ribosomes with the lethal mutations (U56Δ, A1319Δ, and A1319C) are not very active in the overall process of protein synthesis. To understand the basis for the inhibition of protein synthesis, we analyzed the mutant ribosomes for defects in tRNA binding using two approaches. First, we used a toeprinting assay to precisely monitor binding of $tRNA^{fMet}$ to the P site (*44*). Binding of $tRNA^{fMet}$ to the P site produces a reverse transcriptase stop at position +16 of the mRNA, which corresponds to the fraction of mRNA bound to the 30S subunit (Figure 5A). Control experiments showed that in the absence of $tRNA^{fMet}$, no stop is produced at position +16, indicating that the mRNA is not stably bound to the 30S subunit under these conditions (Figure 5A, lane 1). The wild-type 30S subunit showed quantitative binding of $tRNA^{fMet}$ to the P site with a 1.5-fold

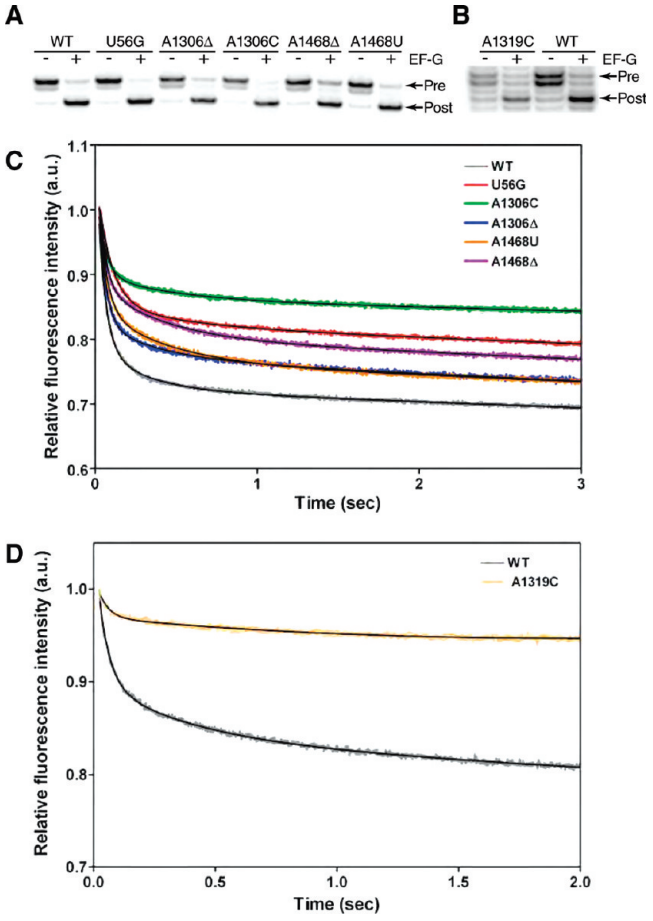

FIGURE 6: Translocation of the mRNA−tRNA complex. (A) The extent of translocation by the mutant ribosomes was determined using the toeprinting assay. Minus and plus signs indicate the absence and presence of EF-G, respectively. Toeprints corresponding to the pretranslocation (Pre) and post-translocation (Post) complexes are indicated. (B) Translocation by affinity-purified wild-type and A1319C ribosomes. (C) Pre-steady state kinetic analysis of EF-G-dependent translocation of wild-type and mutant ribosomes. (D) Translocation kinetics of affinity-purified wild-type and A1319C ribosomes. The decrease in fluorescence intensity corresponds to EF-G-dependent mRNA−tRNA complex translocation and was fit to a double-exponential equation (black line).

Table 2: Pre-Steady State Rates[a] of Translocation by Mutant Ribosomes

ribosome	k_{obs1} (s^{-1})	A_1	k_{obs2} (s^{-1})	A_2
wild type	18.4 ± 0.7	0.32 ± 0.01	2.9 ± 0.4	0.06 ± 0.005
U56G	11.9 ± 0.8	0.21 ± 0.01	2.1 ± 0.5	0.04 ± 0.007
A1306Δ	23.5 ± 0.8	0.33 ± 0.01	2.8 ± 0.3	0.06 ± 0.003
A1306C	20.9 ± 2.7	0.16 ± 0.02	2.3 ± 0.2	0.04 ± 0.005
A1468Δ	24.3 ± 0.7	0.25 ± 0.01	2.5 ± 0.1	0.09 ± 0.002
A1468U	22.0 ± 1.4	0.29 ± 0.02	2.4 ± 0.1	0.09 ± 0.003
wild type[b]	21.3 ± 2.0	0.16 ± 0.01	2.4 ± 0.2	0.07 ± 0.003
A1319C[b]	20.9 ± 2.4	0.04 ± 0.01	0.4 ± 0.1	0.15 ± 0.02

[a] The means ± standard deviations of four experiments are shown. [b] Ribosomes purified using the MS2 affinity tag.

excess of $tRNA^{fMet}$ (Figure 5A, lane 2). Similarly, U56G ribosomes showed no defects in tRNA binding (≈100% bound) (Figure 5C). In contrast, U56Δ mutant 30S subunits did not bind tRNA even with a 10-fold excess of $tRNA^{fMet}$ (≈10% bound) (Figure 5A). A slightly reduced level of $tRNA^{fMet}$ binding was observed with A1306Δ and A1306C (75−80% bound) (Figure 5B). A1319Δ exhibited strong reduction (<10% bound), while A1319C exhibited a smaller reduction in its level of binding of $tRNA^{fMet}$ (≈50% bound) (Figure 5A). Finally, A1468Δ and A1468U showed a slight reduction in their level of binding of $tRNA^{fMet}$ (≈80% bound) (Figure 5B). The second assay that we used was equilibrium tRNA filter binding, and the overall result that we obtained was consistent with that of the toeprinting assay (Figure 5C).

It is known that the 70S ribosome has a higher affinity for tRNA than the 30S subunit. Furthermore, tRNA can stabilize the association of the subunits. Therefore, we repeated the toeprinting experiments in the presence of the 50S subunit. As expected, wild-type ribosomes efficiently bound $tRNA^{fMet}$ at the lowest concentration (Figure 5A, right panel). The U56Δ mutant showed a slight improvement in the presence of the 50S subunit, although the level of binding was still significantly reduced (≈20% bound) (Figure 5A, right panel). However, A1319Δ and A1319C did not show any improvements in binding $tRNA^{fMet}$ (Figure 5A, right panel).

We next performed chemical modification experiments to examine the integrity of the ribosome structure near the tRNA binding sites. Primer extension analysis showed that the overall structure of the 16S rRNA near the tRNA binding sites appears to be similar in wild-type and mutant ribosomes (Figure 4 of the Supporting Information). Differences in the pattern of chemical reactivity of A1319Δ and A1319C compared to that of the wild type were observed in the vicinity of G966 (Figure 4F of the Supporting Information).

Translocation of the mRNA−tRNA Complex. Our studies showed that deletion of U56 or A1319 caused a severe defect in subunit association and tRNA binding, resulting essentially in inactive 30S subunits. Therefore, U56Δ and A1319Δ were not analyzed further; instead, we focused on mutant ribosomes that showed only minor defects in these functional assays. We examined the ability of mutant ribosomes to translocate the mRNA−tRNA complex. Mutant ribosomes purified from *E. coli* strain SQZ10 (Δ7rrn) were analyzed separately from ribosomes purified using the MS2 affinity tag and compared with the appropriate wild-type ribosomes. EF-G-dependent translocation of the mRNA−tRNA complex was monitored initially by the toeprinting assay (*34*, *44*). Translocation of the mRNA−tRNA complex results in the appearance of a toeprint that is three nucleotides shorter compared to the pretranslocation state (Figure 6A,B). The extent of translocation was similar for the wild-type, U56G, A1306Δ, A1306C, A1319C, A1468Δ, and A1468U ribosomes (>90% translocation). These results show that the mutant ribosomes can form authentic pretranslocation complexes and are able to translocate the mRNA−tRNA complex upon addition of EF-G.

To detect any differences in the rate of translocation, we determined the pre-steady state kinetics of mRNA−tRNA complex translocation using a fluorescence-based, stopped-flow method (*45*). Wild-type and mutant ribosomes were used to form pretranslocation complexes, and the translocation rate was determined with a 5-fold excess of EF-G. The time course of translocation showed two phases: a rapid phase ($k_{obs1} \approx 20\ s^{-1}$) followed by a much slower phase ($k_{obs2} \approx 2\ s^{-1}$) (Figure 6C,D). The reason for the slow phase is not known and may be due to sample heterogeneity (*7*). Wild-type, A1306C, A1306Δ, A1468U, and A1468Δ ribosomes translocated the mRNA−tRNA complex with similar rates (Figure 6C and Table 2). In contrast, the rate of translocation by U56G mutant ribosomes ($k_{obs1} = 12\ s^{-1}$)

Table 3: Summary of Defects[a] Caused by Mutations in 16S rRNA

activity	U56Δ	U56G	A1306Δ	A1306C	A1319Δ	A1319C	A1468Δ	A1468U
growth phenotype	lethal	+++	++	++	lethal	lethal	+++	+
polysome profile	ND[b]	+++	++	++	ND[b]	ND[b]	+	+
subunit association	−	ND[b]	ND[b]	ND[b]	−	++++	ND[b]	ND[b]
in vitro translation	−	+++	+++	++++	−	+	++++	++
tRNA binding (P site)	−	++++	+++	+++	−	+++	+++	+++
translocation rate	ND[b]	++	++++	++++	ND[b]	++++[c]	++++	++++

[a] Lethal, does not support growth of *E. coli* strain SQZ10 (Δ7rrn); ++++, no defect; +++, ++, and +, slight to severe defect, where +++ is slight defect; −, no detectable activity. [b] Not determined. [c] The extent of rapid translocation was reduced.

was ≈2-fold lower than that of the wild-type ribosomes (Figure 6C and Table 2). In the case of A1319C ribosomes, the rate of the fast phase was not affected ($k_{obs1} = 21\ s^{-1}$) (Figure 6D and Table 2). However, the amplitude of the fast phase was reduced by 85%, and translocation proceeded mainly by the slow phase ($k_{obs2} = 0.4\ s^{-1}$).

DISCUSSION

Translocation of tRNAs is a complex process involving large-scale structural rearrangements by the ribosome. The rRNAs, which intimately interact with the mRNA and the tRNAs, are likely to play a critical role during translocation. It is often difficult to predict the functional role of specific bases from the high-resolution crystal structures of the ribosomes. We developed a new modification-interference method to identify bases in 16S rRNA that are important for tRNA translocation. The modification-interference method identified 11 bases; six are located in the A site and are protected when tRNA binds (*48*). The bases that are protected by A site tRNA are located in the decoding region of the 30S subunit (Figure 4B) (*49*) and are important for tRNA selection (*39*) and EF-G-dependent translocation (*29*).

In addition to the bases protected by A site tRNA, our modification-interference analysis identified five new bases that may play a role in translocation (Figure 3A). The modification-interference assay relied on chemically modifying the base to inhibit translocation. Chemically modifying a base may not have the same effect as mutating a base, especially when bulky groups are added to the base. Nevertheless, we carried out single-base substitutions and deletion at each of these positions to investigate their role in protein synthesis. Some of the substitutions had no effect on growth rate; in contrast, U56Δ, A1319C, and A1319Δ were unable to support the growth of *E. coli* strain SQZ10 (Δ7rrn) (summarized in Table 3). Insights into the possible role of these five bases in translation are discussed below.

The 30S subunit from U56Δ is missing several r-proteins and is inactive in subunit association. In addition, U56Δ ribosomes are unable to bind tRNA and translate a reporter protein in vitro. These results are consistent with the inability of U56Δ to replace the resident wild-type plasmid in *E. coli* strain SQZ10 (Δ7rrn). In contrast, U56G is able to support the growth of *E. coli* strain SQZ10 (Δ7rrn) at a reduced growth rate. U56G appears to be normal in polysome formation, r-protein content, and tRNA binding. Interestingly, U56G exhibited a 2-fold reduction in the rate of translocation (Figure 6C and Table 2). Nucleotide U56 is universally conserved among all three phylogenetic kingdoms (*50*) and is located in helix 5 within the body of the 30S subunit (Figure 3B) (*51*). This region of the 16S rRNA was cleaved by hydroxyl radicals emanating from Fe-EDTA tethered to amino acids 37 and 65 within domain II of EF-G in the fusidic acid-stabilized post-translocation complex (*52*). In addition, positions 55 and 57 in 16S rRNA are protected from hydroxyl radicals in both the EF-G·GDPNP complex and the fusidic acid-stabilized complex (*53*). These results are in agreement with cryo-EM studies, which showed that domain II of EF-G interacts with helix 5 (*14*). Modification by CMCT adds the bulky CMC group at the N3 position of U56, which may interfere with EF-G binding or activity.

Position U723 is a bulged nucleotide located in helix 23a within the platform of the 30S subunit (Figure 3B). It is selectively conserved in bacteria and archaea (> 90% conserved) (*50*). Our studies showed that mutation or deletion of U723 does not affect the growth rate, indicating that the base is not essential for translation. However, it is interesting that U723 interacts with the minor groove of the Shine-Dalgarno (SD) helix (Figure 3C) (*54*, *55*). Modification of U723 by CMCT may cause a steric clash with the SD helix and inhibit the movement of the mRNA during translocation. This may explain why modification at U723 is underrepresented in the selected population.

Positions A1306 and A1319 are conserved residues (>98% conservation) located in helix 42 within the head of the 30S subunit (Figure 3B) (*51*, *56*). A1306Δ and A1306C exhibited reduced growth rates, defects in polysome formation, and a slight inhibition of binding tRNA. However, the rate of translocation was not decreased in A1306Δ and A1306C (Table 2). In contrast, deletion of A1319 is lethal, and the mutant 30S subunits fail to associate with the 50S subunit. Furthermore, A1319Δ binds tRNA poorly and is inactive in protein synthesis. Similarly, A1319C is also lethal, but the mutant 30S subunit is able to associate with the 50S subunit, is able to bind tRNA with better efficiency, and is partially active in proteins synthesis in vitro. Interestingly, A1319C exhibited an 85% decrease in the amplitude of the fast phase of translocation, indicating that the extent of translocation was reduced. This decrease may be caused by a reduced level of tRNA binding [≈50% reduction in the level of tRNA binding (Figure 5)]. This interpretation is consistent with toeprinting experiments, which showed reduced levels of pre- and post-translocation complexes compared to the wild-type ribosomes (in Figure 6B, compare intensities for "Pre" and "Post" bands). Cryo-EM studies showed that the largest conformational change during translocation occurs in the 30S head domain, especially in helices 39, 41, and 42 of 16S rRNA (*57*, *58*). Therefore, we speculate that chemical modification of bases A1306 and A1319 in helix 42 of 16S rRNA may inhibit the conformational changes that occur during translocation, resulting in the modification being underrepresented in the selected population.

Position A1468 is a universally conserved residue located in helix 44 of 16S rRNA (Figure 3). This helix lies at the subunit interface and makes extensive contacts with the 50S subunit

(*56*, *59*−*61*). Our results show that A1468Δ and A1468U have reduced growth rates and defects in polysome formation (Table 3). However, A1468Δ and A1468U appeared normal in tRNA binding and in the rate of translocation. These results suggest that A1468 is important for subunit association in vivo. Base A1468 is in an internal loop of helix 44, and the opposite strand of this loop (positions 1429−1433) forms part of bridge B6 (*57*). In addition, bases 1433 and 1434 form tertiary interactions with bases 319−335 in helix 13 (Figure 3E) (*56*, *60*, *61*). The defect in subunit association may result from the A1468U mutation forming a base pair with one of the nucleotides in the opposite strand of the loop (AGAA), thereby disrupting bridge B6. Alternatively, the A1468U mutation may cause a structural perturbation that misaligns helix 44 relative to the rest of the 30S subunit, thereby weakening its association with the 50S subunit. Cryo-EM studies indicate that the small and large ribosomal subunits undergo a ratchet-like rotation (RSR) relative to each other during translocation (*57*, *58*). The pivot axis for the RSR is located close to A1468. It is possible that chemical modification of A1468 may interfere with the coordinated movement of the two subunits relative to each other during translocation.

ACKNOWLEDGMENT

We thank Ulrich Muller, Byron Hetrick, and Prashant Khade for helpful comments on the manuscript.

SUPPORTING INFORMATION AVAILABLE

Data showing site-specific cross-linking of *E. coli* $tRNA_1^{Val}$ to 16S rRNA, translocation of 3′-biotin-$tRNA_1^{Val}$ from the A site, analysis of ribosomal proteins present in mutant subunits by two-dimensional gel electrophoresis, in vitro protein synthesis by mutant ribosomes, structural changes in 16S rRNA of the mutant ribosomes, and primer extension analysis of 30S subunits purified using the MS2 affinity tag. This material is available free of charge via the Internet at http://pubs.acs.org.

REFERENCES

1. Moazed, D., and Noller, H. F. (1989) Intermediate states in the movement of transfer RNA in the ribosome. *Nature 342*, 142–148.
2. Odom, O. W., Picking, W. D., and Hardesty, B. (1990) Movement of tRNA but not the nascent peptide during peptide bond formation on ribosomes. *Biochemistry 29*, 10734–10744.
3. Rodnina, M. V., Savelsbergh, A., Katunin, V. I., and Wintermeyer, W. (1997) Hydrolysis of GTP by elongation factor G drives tRNA movement on the ribosome. *Nature 385*, 37–41.
4. Dorner, S., Brunelle, J. L., Sharma, D., and Green, R. (2006) The hybrid state of tRNA binding is an authentic translation elongation intermediate. *Nat. Struct. Mol. Biol. 13*, 234–241.
5. Pan, D., Kirillov, S. V., and Cooperman, B. S. (2007) Kinetically competent intermediates in the translocation step of protein synthesis. *Mol. Cell 25*, 519–529.
6. Ermolenko, D. N., Spiegel, P. C., Majumdar, Z. K., Hickerson, R. P., Clegg, R. M., and Noller, H. F. (2007) The antibiotic viomycin traps the ribosome in an intermediate state of translocation. *Nat. Struct. Mol. Biol. 14*, 493–497.
7. Walker, S. E., Shoji, S., Pan, D., Cooperman, B. S., and Fredrick, K. (2008) Role of hybrid tRNA-binding states in ribosomal translocation. *Proc. Natl. Acad. Sci. U.S.A. 105*, 9192–9197.
8. Julian, P., Konevega, A. L., Scheres, S. H., Lazaro, M., Gil, D., Wintermeyer, W., Rodnina, M. V., and Valle, M. (2008) Structure of ratcheted ribosomes with tRNAs in hybrid states. *Proc. Natl. Acad. Sci. U.S.A. 105*, 16924–16927.
9. Agirrezabala, X., Lei, J., Brunelle, J. L., Ortiz-Meoz, R. F., Green, R., and Frank, J. (2008) Visualization of the hybrid state of tRNA binding promoted by spontaneous ratcheting of the ribosome. *Mol. Cell 32*, 190–197.
10. Spiegel, P. C., Ermolenko, D. N., and Noller, H. F. (2007) Elongation factor G stabilizes the hybrid-state conformation of the 70S ribosome. *RNA 13*, 1473–1482.
11. Agrawal, R. K., Heagle, A. B., Penczek, P., Grassucci, R. A., and Frank, J. (1999) EF-G-dependent GTP hydrolysis induces translocation accompanied by large conformational changes in the 70S ribosome. *Nat. Struct. Biol. 6*, 643–647.
12. Frank, J., and Agrawal, R. K. (2000) A ratchet-like inter-subunit reorganization of the ribosome during translocation. *Nature 406*, 318–322.
13. Stark, H., Rodnina, M. V., Wieden, H. J., van Heel, M., and Wintermeyer, W. (2000) Large-scale movement of elongation factor G and extensive conformational change of the ribosome during translocation. *Cell 100*, 301–309.
14. Connell, S. R., Takemoto, C., Wilson, D. N., Wang, H., Murayama, K., Terada, T., Shirouzu, M., Rost, M., Schuler, M., Giesebrecht, J., Dabrowski, M., Mielke, T., Fucini, P., Yokoyama, S., and Spahn, C. M. (2007) Structural basis for interaction of the ribosome with the switch regions of GTP-bound elongation factors. *Mol. Cell 25*, 751–764.
15. Cundliffe, E. (1990) in The Ribosome. Structure, Function, and Evolution (Hill, W. E., Dahlberg, A., Garrett, R. A., Moore, P. B., Schlessinger, D., and Warner, J. R., Eds.) pp 479−490, American Society for Microbiology, Washington, DC.
16. Thompson, J., Cundliffe, E., and Dahlberg, A. E. (1988) Site-directed mutagenesis of *Escherichia coli* 23 S ribosomal RNA at position 1067 within the GTP hydrolysis centre. *J. Mol. Biol. 203*, 457–465.
17. Rosendahl, G., and Douthwaite, S. (1994) The antibiotics micrococcin and thiostrepton interact directly with 23S rRNA nucleotides 1067A and 1095A. *Nucleic Acids Res. 22*, 357–363.
18. Moazed, D., and Noller, H. F. (1987) Interaction of antibiotics with functional sites in 16S ribosomal RNA. *Nature 327*, 389–394.
19. Moazed, D., and Noller, H. F. (1987) Chloramphenicol, erythromycin, carbomycin and vernamycin B protect overlapping sites in the peptidyl transferase region of 23S ribosomal RNA. *Biochimie 69*, 879–884.
20. Carter, A. P., Clemons, W. M., Brodersen, D. E., Morgan-Warren, R. J., Wimberly, B. T., and Ramakrishnan, V. (2000) Functional insights from the structure of the 30S ribosomal subunit and its interactions with antibiotics. *Nature 407*, 340–348.
21. Brodersen, D. E., Clemons, W. M., Jr., Carter, A. P., Morgan-Warren, R. J., Wimberly, B. T., and Ramakrishnan, V. (2000) The structural basis for the action of the antibiotics tetracycline, pactamycin, and hygromycin B on the 30S ribosomal subunit. *Cell 103*, 1143–1154.
22. Harms, J. M., Wilson, D. N., Schluenzen, F., Connell, S. R., Stachelhaus, T., Zaborowska, Z., Spahn, C. M., and Fucini, P. (2008) Translational regulation via L11: Molecular switches on the ribosome turned on and off by thiostrepton and micrococcin. *Mol. Cell 30*, 26–38.
23. Borovinskaya, M. A., Shoji, S., Holton, J. M., Fredrick, K., and Cate, J. H. (2007) A steric block in translation caused by the antibiotic spectinomycin. *ACS Chem. Biol. 2*, 545–552.
24. Moazed, D., Robertson, J. M., and Noller, H. F. (1988) Interaction of elongation factors EF-G and EF-Tu with a conserved loop in 23S RNA. *Nature 334*, 362–364.
25. Skold, S. E. (1983) Chemical crosslinking of elongation factor G to the 23S RNA in 70S ribosomes from *Escherichia coli*. *Nucleic Acids Res. 11*, 4923–4932.
26. Lill, R., Robertson, J. M., and Wintermeyer, W. (1989) Binding of the 3′ terminus of tRNA to 23S rRNA in the ribosomal exit site actively promotes translocation. *EMBO J. 8*, 3933–3938.
27. Feinberg, J. S., and Joseph, S. (2001) Identification of molecular interactions between P site tRNA and the ribosome essential for translocation. *Proc. Natl. Acad. Sci. U.S.A. 98*, 11120–11125.
28. Phelps, S. S., Jerinic, O., and Joseph, S. (2002) Universally conserved interactions between the ribosome and the anticodon stem-loop of A site tRNA important for translocation. *Mol. Cell 10*, 799–807.
29. Garcia-Ortega, L., Stephen, J., and Joseph, S. (2008) Precise alignment of peptidyl tRNA by the decoding center is essential for EF-G-dependent translocation. *Mol. Cell 32*, 292–299.
30. von Ahsen, U., and Noller, H. F. (1995) Identification of bases in 16S rRNA essential for tRNA binding at the 30S ribosomal P site. *Science 267*, 234–237.
31. Yoshizawa, S., Fourmy, D., and Puglisi, J. D. (1999) Recognition of the codon-anticodon helix by ribosomal RNA. *Science 285*, 1722–1725.
32. Bocchetta, M., Xiong, L., and Mankin, A. S. (1998) 23S rRNA positions essential for tRNA binding in ribosomal functional sites. *Proc. Natl. Acad. Sci. U.S.A. 95*, 3525–3530.

33. Stern, S., Moazed, D., and Noller, H. F. (1988) Structural analysis of RNA using chemical and enzymatic probing monitored by primer extension. *Methods Enzymol. 164*, 481–489.
34. Joseph, S., and Noller, H. F. (1998) EF-G-catalyzed translocation of anticodon stem-loop analogs of transfer RNA in the ribosome. *EMBO J. 17*, 3478–3483.
35. Youngman, E. M., Brunelle, J. L., Kochaniak, A. B., and Green, R. (2004) The active site of the ribosome is composed of two layers of conserved nucleotides with distinct roles in peptide bond formation and peptide release. *Cell 117*, 589–599.
36. Asai, T., Condon, C., Voulgaris, J., Zaporojets, D., Shen, B., Al-Omar, M., Squires, C., and Squires, C. L. (1999) Construction and initial characterization of *Escherichia coli* strains with few or no intact chromosomal rRNA operons. *J. Bacteriol. 181*, 3803–3809.
37. Asai, T., Zaporojets, D., Squires, C., and Squires, C. L. (1999) An *Escherichia coli* strain with all chromosomal rRNA operons inactivated: Complete exchange of rRNA genes between bacteria. *Proc. Natl. Acad. Sci. U.S.A. 96*, 1971–1976.
38. Ron, E. Z., Kohler, R. E., and Davis, B. D. (1966) Polysomes extracted from *Escherichia coli* by freeze-thaw-lysozyme lysis. *Science 153*, 1119–1120.
39. Cochella, L., Brunelle, J. L., and Green, R. (2007) Mutational analysis reveals two independent molecular requirements during transfer RNA selection on the ribosome. *Nat. Struct. Mol. Biol. 14*, 30–36.
40. Bartetzko, A., and Nierhaus, K. H. (1988) Mg^{2+}/NH_4^+/polyamine system for polyuridine-dependent polyphenylalanine synthesis with near in vivo characteristics. *Methods Enzymol. 164*, 650–658.
41. Dabrowski, M., Spahn, C. M., Schafer, M. A., Patzke, S., and Nierhaus, K. H. (1998) Protection patterns of tRNAs do not change during ribosomal translocation. *J. Biol. Chem. 273*, 32793–32800.
42. Nierhaus, K. (1990) in Ribosomes and Protein Synthesis: A Practical Approach (Spedding, G., Ed.) pp 161−189, IRL Press, Oxford, U.K.
43. Geyl, D., Bock, A., and Isono, K. (1981) An improved method for two-dimensional gel-electrophoresis: Analysis of mutationally altered ribosomal proteins of *Escherichia coli*. *Mol. Gen. Genet. 181*, 309–312.
44. Hartz, D., McPheeters, D. S., Traut, R., and Gold, L. (1988) Extension inhibition analysis of translation initiation complexes. *Methods Enzymol. 164*, 419–425.
45. Studer, S. M., Feinberg, J. S., and Joseph, S. (2003) Rapid Kinetic Analysis of EF-G-dependent mRNA Translocation in the Ribosome. *J. Mol. Biol. 327*, 369–381.
46. Schwartz, I., and Ofengand, J. (1978) Photochemical cross-linking of unmodified acetylvalyl-tRNA to 16S RNA at the ribosomal P site. *Biochemistry 17*, 2524–2530.
47. Ofengand, J., Liou, R., Kohut, J., Schwartz, I., and Zimmermann, R. A. (1979) Covalent cross-linking of transfer ribonucleic acid to the ribosomal P site. Mechanism and site of reaction in transfer ribonucleic acid. *Biochemistry 18*, 4322–4332.
48. Moazed, D., and Noller, H. F. (1986) Transfer RNA shields specific nucleotides in 16S ribosomal RNA from attack by chemical probes. *Cell 47*, 985–994.
49. Ogle, J. M., Brodersen, D. E., Clemons, W. M., Jr., Tarry, M. J., Carter, A. P., and Ramakrishnan, V. (2001) Recognition of cognate transfer RNA by the 30S ribosomal subunit. *Science 292*, 897–902.
50. Cannone, J. J., Subramanian, S., Schnare, M. N., Collett, J. R., D'Souza, L. M., Du, Y., Feng, B., Lin, N., Madabusi, L. V., Muller, K. M., Pande, N., Shang, Z., Yu, N., and Gutell, R. R. (2002) The Comparative RNA Web (CRW) Site: An online database of comparative sequence and structure information for ribosomal, intron, and other RNAs. *BMC Bioinf. 3*, 2.
51. Wimberly, B. T., Brodersen, D. E., Clemons, W. M., Jr., Morgan-Warren, R. J., Carter, A. P., Vonrhein, C., Hartsch, T., and Ramakrishnan, V. (2000) Structure of the 30S ribosomal subunit. *Nature 407*, 327–339.
52. Wilson, K. S., and Noller, H. F. (1998) Mapping the position of translational elongation factor EF-G in the ribosome by directed hydroxyl radical probing. *Cell 92*, 131–139.
53. Wilson, K. S., and Nechifor, R. (2004) Interactions of translational factor EF-G with the bacterial ribosome before and after mRNA translocation. *J. Mol. Biol. 337*, 15–30.
54. Korostelev, A., Trakhanov, S., Asahara, H., Laurberg, M., Lancaster, L., and Noller, H. F. (2007) Interactions and dynamics of the Shine Dalgarno helix in the 70S ribosome. *Proc. Natl. Acad. Sci. U.S. A. 104*, 16840–16843.
55. Kaminishi, T., Wilson, D. N., Takemoto, C., Harms, J. M., Kawazoe, M., Schluenzen, F., Hanawa-Suetsugu, K., Shirouzu, M., Fucini, P., and Yokoyama, S. (2007) A snapshot of the 30S ribosomal subunit capturing mRNA via the Shine-Dalgarno interaction. *Structure 15*, 289–297.
56. Schuwirth, B. S., Borovinskaya, M. A., Hau, C. W., Zhang, W., Vila-Sanjurjo, A., Holton, J. M., and Cate, J. H. (2005) Structures of the bacterial ribosome at 3.5 Å resolution. *Science 310*, 827–834.
57. Gao, H., Sengupta, J., Valle, M., Korostelev, A., Eswar, N., Stagg, S. M., Van Roey, P., Agrawal, R. K., Harvey, S. C., Sali, A., Chapman, M. S., and Frank, J. (2003) Study of the structural dynamics of the *E. coli* 70S ribosome using real-space refinement. *Cell 113*, 789–801.
58. Valle, M., Zavialov, A., Sengupta, J., Rawat, U., Ehrenberg, M., and Frank, J. (2003) Locking and unlocking of ribosomal motions. *Cell 114*, 123–134.
59. Yusupov, M. M., Yusupova, G. Z., Baucom, A., Lieberman, K., Earnest, T. N., Cate, J. H. D., and Noller, H. F. (2001) Crystal Structure of the Ribosome at 5.5 Å Resolution. *Science 292*, 883–896.
60. Korostelev, A., Trakhanov, S., Laurberg, M., and Noller, H. F. (2006) Crystal structure of a 70S ribosome-tRNA complex reveals functional interactions and rearrangements. *Cell 126*, 1065–1077.
61. Selmer, M., Dunham, C. M., Murphy, F. V. t., Weixlbaumer, A., Petry, S., Kelley, A. C., Weir, J. R., and Ramakrishnan, V. (2006) Structure of the 70S ribosome complexed with mRNA and tRNA. *Science 313*, 1935–1942.